CHALMERS
UNIVERSITY OF TECHNOLOGY

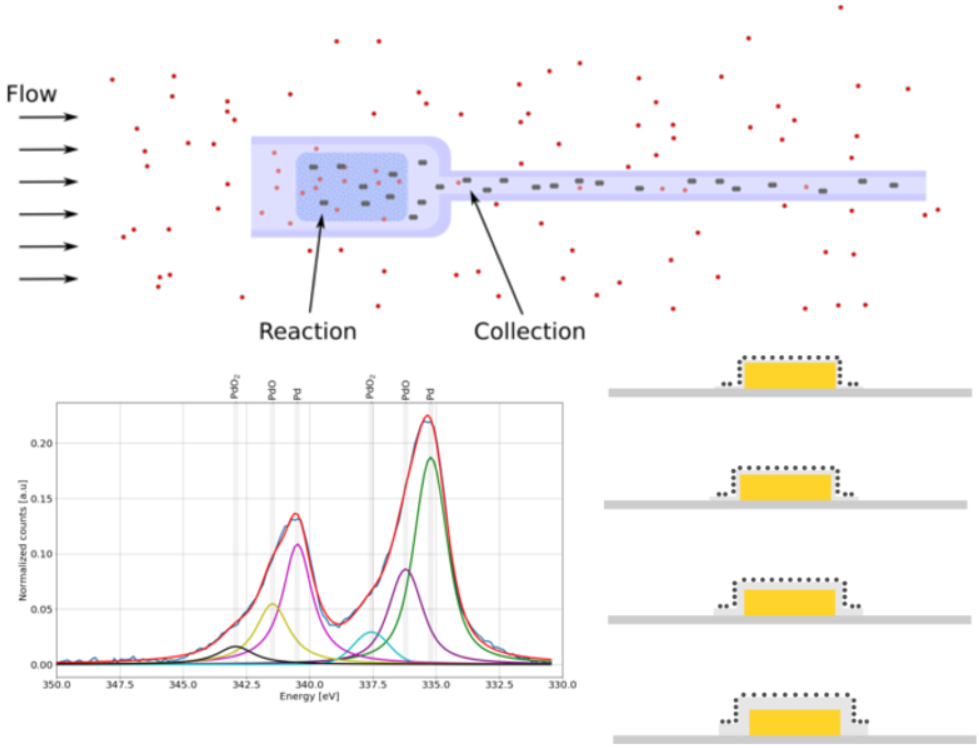

Improvements to a flow reactor and catalysis on core shell nanoparticles

Master's thesis in Applied Physics

JOHAN TENGHAMN

Department of Physics
CHALMERS UNIVERSITY OF TECHNOLOGY
Gothenburg, Sweden 2018

Master's thesis 2017:NN

Improvements to a flow reactor and catalysis on core shell nanoparticles

Johan Tenghamn

CHALMERS
UNIVERSITY OF TECHNOLOGY

Department of Physics
Division of Chemical Physics
Chalmers University of Technology
Gothenburg, Sweden 2018

Improvements to a flow reactor and catalysis on core shell nanoparticles
Johan Tenghamn

Supervisors: Stephan Bartling and Arturo Susarrey-Arce, Department of Physics
Examiner: Christoph Langhammer, Department of Physics

Master's Thesis 2018:NN
Department of Physics
Division of Chemical Physics
Chalmers University of Technology
SE-412 96 Gothenburg
Telephone +46 31 772 1000

Chalmers Reproservice
Gothenburg, Sweden 2018

Improvements to a flow reactor and catalysis on core shell nanoparticles
Johan Tenghamn
Department of Physics
Chalmers University of Technology

Abstract

A flow reactor is a common measurement equipment in catalysis research and works by flowing reactants into a reactor/reservoir and measuring the outgoing products. At the Langhammer lab at Chalmers University of Technology there is a flow reactor developed mainly for research in plasmonic sensing where the outgoing gas was not analysed in detail. Now when used for catalysis research there was a need for improving the detection of outgoing species. By introducing a glass pocket sample holder that encapsulates the sample we reduced dilution and improved the signal by two orders of magnitude. This improvement is presented and tested with the test reaction CO oxidation.
Samples cotaining novel type of supported core shell nanoparticles with gold core, alumina shell covered with either catalytic Pd or Pt particles was then tested. By varying the shell thickness between 0 and 5 nm we studied the influence on CO oxidation by comparing activation energies. Similar trends for reactions in low CO concentrations (5 % vol CO) for both Pd and Pt samples but different trends for high CO (50 % vol CO) was obtained. XPS measurements indicates that the formation Pd oxides could be influenced by the shell thickness. A possible explanation could be an effect from Fermi level equilibration and charge transfer between the core and the catalysts but this needs to be confirmed with further measures varying for example the core material.

Keywords: flow reactor, catalysis, core shell, CO, oxidation, activation energy, nanoparticles, Fermi level equilibration, XPS, SEM, pocket reactor.

Acknowledgements

I would like to start thank the entire the Chemical physics division. It has been great spending time here, never thought that it would be so much fun doing a thesis project. So many people with so much knowledge, always open for discussions when questions appearing.
To be more specific, I would like to give a huge thanks to both my supervisors Stephan Bartling and Arturo Susarrey-Arce. Both have been pushing me in my experiments, giving me suggestions, spent time to discuss and explain. They have always been giving me feedback in a very positive way.
I would also like to give a huge thanks to my office friend Christopher Tiburski. We have analysed and discussed a lot of data. Together we have developed the *ttlab* software[1] used for all the data analysis in this thesis.
Thanks to Christoph Langhammer my examiner for giving me the opportunity of doing this project.

Johan Tenghamn, Gothenburg, August 2018

Contents

List of Figures

1

Introduction

”Patience is a virtue” is a famous saying originating from a poem called Piers Plowman written around 1360 by the English poet William Langland[2]. If this saying always is true can though be debated. Just waiting for the environmental pollution to stop, hoping for the polar ices to start increasing their area again and waiting for the be likely toxic smog in the big cities to decrease is probably not the best approach.

This thesis report will not deal with the environmental problems themselves nor will it present any solutions to them. It will however focus on the very important concept of catalysts, a concept probably popular amongst the impatient. Which can be used both to reduce energy consumption and emission of toxic gases. By definition, a catalyst is a material that increases the rate of chemical reactions by participating in the reactions but is left unchanged when the reaction is over[3].

This is not a new concept, it has been attracting interest for a long time, two of the first scientific findings dates back to 1800 where dehydrogenation of ethyl alcohol over metal catalysts was reported independently by both Joseph Priestly and Martinus van Marum[4]. The earliest use of catalysts dates though much further back than that. One example being the use of yeast which contains an enzyme increasing the fermentation of sugar from grains and fruits to give out alcohol which has been known for at least 8000 years.

Today, the research field of catalysis can be divided in several different sub-fields and the number of different reactions studied are many[5, 6]. The research can be both for environmental causes and for understanding the basic mechanisms behind the increased reaction rate and it usually consists of utilising state of the art fabrication techniques and several spectroscopy techniques to characterise the catalysts[7].

In this thesis you will read about improvements to a flow reactor used to study catalysts but also an investigation of catalysis on a specific type of nanoparticles called core shell nanoparticles. The ideas of improving the flow reactor origins from previous work by Hans O. A. Fredriksson et. al [8] and reduced the dilution of catalyst products in a flow reactor by encapsulating a sample in a glass pocket. The core shell nanoparticles has been developed here at Chalmers mainly by Arturo Susarrey-Arce and earlier master thesis project by Iwan Darmadi[9]. Both a characterisation of the these, using x-ray photoelectron spectroscopy (XPS), scanning electron microscopy (SEM) and optical spectroscopy as well as determining the catalytic activity of CO oxidation using the improved flow reactor will be covered.

1.1 Background to the flow reactor improvements

A flow reactor is a commonly used equipment when studying catalysis. It usually consists of some kind of reservoir in which one can flow either gases or liquids into and let them chemically react. By controlling the flow rate, the gas mixture and the temperature and at the same time measuring what comes out of it one can draw conclusions about what chemical reactions occurs, at what rate and its temperature dependency. In the lab at Chemical Physics at Chalmers University of Technology there exists a flow reactor used for catalysis measurements. An illustration of it can be seen in figure 1.1. It consists of a glass tube in which reactions occurs and has a sample holder for catalytic samples. The gas inlet is connected to mass flow controllers for controlling gas mixtures and flow rates into the reactor. The outlet connection is connected to a mass spectrometer (MS) with which one can detect and measure outgoing species (we name the outlet connection here to the ”sniffer” since it somewhat resemble a nose trying to sniff up catalytic products). A heating coil and thermocouples are used for changing and measuring the temperature, all controlled with a LabView script.

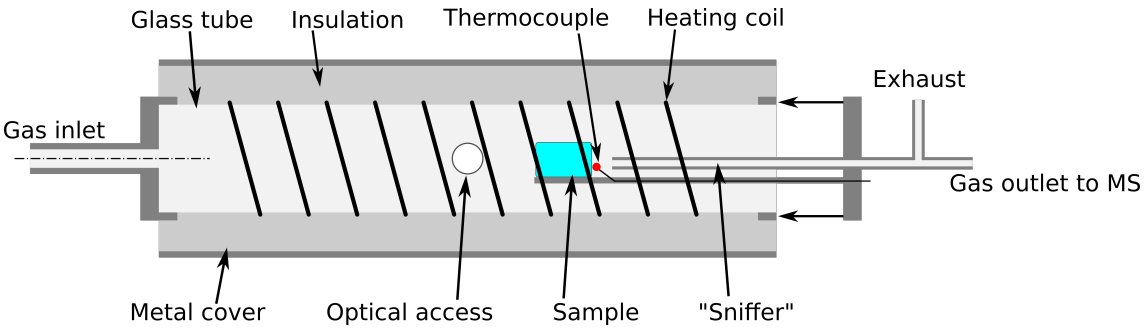

Figure 1.1: Illustration of the initial flow reactor used for catalysis measurements at Chemical physics at Chalmers. The sample typically contains the catalyst of interest.

This setup was mainly developed for plasmonic sensing where the outgoing gas was not analysed in detail. Therefore there was no optimisation of detecting outgoing products. This has resulted in a poor signal of catalytic products.

The cause of this poor signal can be traced to the dilution of the reaction products that occurs between the sample and the MS as illustrated in figure 1.2 a. To reduce this dilution Fredriksson et al encapsulated the sample in a glass holder as illustrated in figure 1.2 b. There is then not much room for dilution, all reactants must travel close to the sample before going into the mass spectrometer.

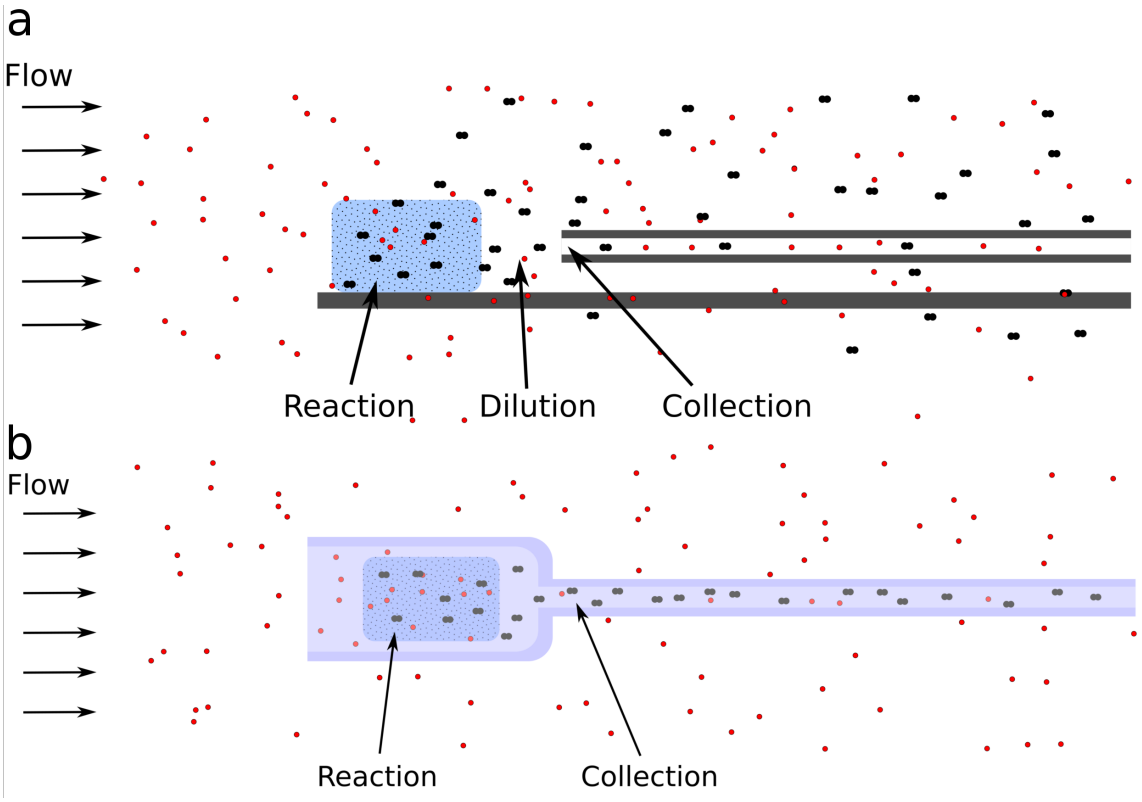

Figure 1.2: **a**) Illustration of the dilution of reaction products that occurs in the reactor. The reactant (red dots) reacts on the sample and forms the product (black double dots). While travelling between the sample and the collection tube it gets diluted with the reactants. **b**) Illustration of the improvement introduced by Fredriksson et al. The sample is encapsulated in a pocket made out of glass. The products goes straight out to the collection and dilution is minimised.

1.2 Catalytic core shell nanoparticles

The core shell nanoparticles developed by Arturo Susarrey-Arce et al. has a cylindrical metal core supported on a substrate covered in a thin shell with catalytic particles deposited on top. This is illustrated in figure 1.3 where one can see the cross section of a core shell nanoparticle. The fabrication method of these is very versatile and allows freely to alternate size and material of the core, the shell and the catalyst. All which in theory can effect the catalytic activity.

In this thesis substrates covered with core-shell nanoparticles with a gold core of 80 nm and an aluminium oxide shell has been investigated. The samples was fabricated with shell thicknesses between 0 nm and 6 nm with two different catalysts, Pt and Pd. The thought mechanism affected by the shell-thickness is Fermi level equilibration via electrons transfer between the core and the catalyst particles. The background theory of this will be covered and the experimental techniques used will be explained. The report will end with an outlook for future investigations.

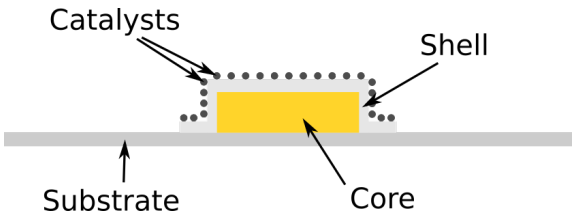

Figure 1.3: An illustration of a core shell nanoparticle in cross section. The core is covered with a thin shell that has catalytic particles on top.

2

Background Theory

2.1 Heterogeneous catalysis

A catalyst is a material that by definition participates in chemical reactions, it increases the reaction rate but is left unchanged after the reaction is over[3]. This possibility of increasing reaction rates has an significant impact on our daily lives. One example is the agriculture industry which is highly dependent on Nitrogen fertilisers which are produced using ammonia. The ammonia is synthesised through a catalytic process called the Haber-Bosch process, which has reduced the energy cost with roughly 75 %[5]. Another example is the automotive exhaust, helping in reducing poisonous gases as carbon monoxides hydrocarbons and nitrogen oxides[10]. The way catalysts work is by reducing the energy barrier for the reaction to occur. This is typically illustrated as in figure 2.1 where the catalyst lowers the activation energy or energy barrier. The occurrence of a reaction from a macroscopic point of view can then typically be seen as a statistical process. How many of the reactants posses enough energy to overcome the energy barrier and how often does the reactants meet?

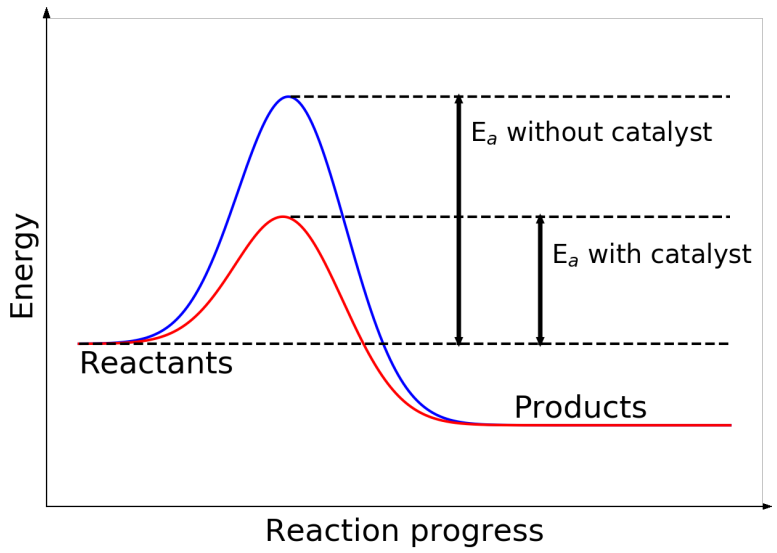

Figure 2.1: The blue graph represents the energy barrier that the reactants need to overcome for the reaction to occur and form the products. With a catalyst, the energy barrier is lowered, represented by the red graph. This lowered energy barrier will result in a higher reaction rate.

In the field of catalysis one often distinguishes between homogeneous and heterogeneous catalysis. In homogeneous catalysis, the catalyst is in the same phase as the reacting species, while in a heterogeneous catalysis the catalyst is in a different phase. Notice that the experiments and results in this report will only be related to heterogeneous catalysis on metal surfaces and therefor no theory of homogeneous catalysis will be covered. Specifically the oxidation of carbon monoxide oxidation on palladium and platinum particles will be addressed.

2.1.1 CO oxidation on Pd and Pt catalysts

The chemical reaction

$$2\,CO + O_2 \longrightarrow 2\,CO_2 \tag{2.1}$$

also known as carbon monoxide oxidation is a frequently studied reaction [11]. It has the advantage of being seemingly a simple reaction, but it is also interesting from an environmental perspective where the pollution of air with CO is considered potentially linked to learning and behavioural abnormalities in children and in higher concentrations very toxic[12]. The most commonly known catalyst for CO oxidation is probably the three-way catalyst used in automotive exhausts.
On Pd and Pt catalysts CO can be oxidised in several ways[11]. In the Langmuir-Hinshelwood mechanism both CO and O_2 adsorbs to the catalyst surface. The O_2 dissociates to two O atoms which can react with the CO and form CO_2 which in turn desorbs from the surface. In the Eley-Rideal mechanism CO in gas phase collides with the surface and reacts directly with an adsorbed O atom. When the reaction conditions are rich in oxygen a third mechanism is also considered present, the Mars-van Krevelen mechanism in which surface oxides are created and in turn is consumed by CO-molecules forming CO_2.
The catalytic activity of Pd and Pt can be surface dependent, e.g. the catalytic activity on the Pd(111) surface is different from the Pd(100) and so on [11]. This is a result of the different distance between atoms on these surfaces and the free energy is therefor also different.

2.1.2 What determines the activity of metals?

There are several parameters determining the activity of a metal. The surface structure is important, adsorption is typically more likely to be hindered on close packed surfaces of metals and the presence of structural defects can lead to increased reactivity[5]. The electronic state is also important, it has been shown that the center of the d-band of transition metals correlates with the interaction strength of chemisorbed O[5]. This is shown in figure 2.2 where in the top figure the interaction strength of chemisorbed O against transition metals. The center of the d-band moves further below the Fermi level when going from left to right in the top figure. In the lower figure the interaction strength is plotted against the center of the d-band with respect to the Fermi level. Zirconium can then be found as the points furthest to the right in the lower figure and Silver as the points furthest to the left. Both experimental and theoretical simulated values are plotted in the figure.

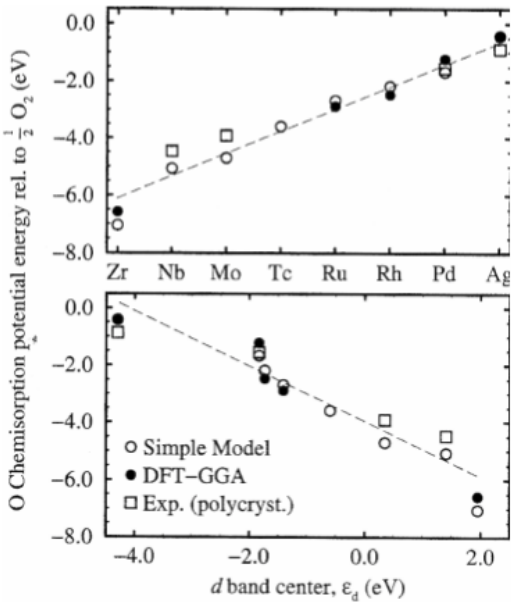

Figure 2.2: In the top figure, interaction strength of chemisorbed oxygen is plotted against transition metals. In the lower figure the interaction strength is plotted against the center of the d-band with respect to the Fermi level. Image taken from *Surface science: foundations of catalysis and nanoscience*[5].

2.1.3 Arrhenius equation, temperature effect on reaction rate

The Arrhenius equation is an equation describing the effect of temperature on chemical reactions. It was first proposed by Hood in 1878, then later on, van't Hoff and Arrhenius gave it more physical relevance [13]. The equation has the form

$$k = A \exp\left(-\frac{E_a}{k_B T}\right) \tag{2.2}$$

where k is the reaction rate, E_a is the activation energy, k_B is the Boltzmann constant and A the pre-exponential factor usually called frequency factor or the Arrhenius factor. The exponential term comes from the Maxwell-Boltzmann energy distribution among particles in a gas and is related to the fraction of particles that possesses enough kinetic energy to overcome the energetic barrier needed for the reaction to occur. The frequency factor or Arrhenius factor can be related to the number of collisions between the reactants per time unit[6].

Determining activation energy and Arrhenius factor from experiments

Typically during catalysis measurements one can either measure the amount of catalysis products directly or some property which is proportional to the amount of product. As an example, a quadrupole mass spectrometer ionises gases and measures the ion current produced by the ionised species. The ioniser has a chance of ionising the species by some probability p, so when comparing two ion currents one needs

to compensate for this probability. The activation energy in Arrhenius equation is though not affected by this probability. This can be understood by looking at what we measure, the rate k times some probability p, $I = k \cdot p$. So we have

$$\frac{I}{p} = A \exp\left(-\frac{E_a}{k_B T}\right) \tag{2.3}$$

Taking the logarithm of this gives

$$\ln(I) - \ln(p) = \ln(A) - \frac{E_a}{k_b T}, \tag{2.4}$$

and by rearranging the terms to

$$\ln(I) = -\frac{E_a}{k_b}\frac{1}{T} + \ln(p) + \ln(A) \tag{2.5}$$

one can see that plotting the ion current I versus the inverse temperature $\frac{1}{T}$, the activation energy divided by Boltzmanns constant is the slope of the curve. p only affects where the slope crosses the y-axis.

2.2 Band structure of solids

The theory of Band structures in Solid State Physics is an important model that helps us understand why some materials behaves as metals with high conductivity while others behave as semiconductors or as insulators. In principle it describes energy regions where the electrons of solids are either allowed (energy bands) or not allowed (band gaps). In figure 2.3 one can see four common types of material and their associated band structure model. The insulator has no electrons in the conduction band and one needs to add a lot of energy to excite electrons to the conduction band. The metal on the other hand, already has electrons in the conduction band at room temperature and the electrons travels easily in the material. The semiconductor to the left has electrons in the conduction band depending on temperature, close to absolute zero it becomes an insulator. The semiconductor to the right shows the energy bands of an electron-deficient semiconductor.

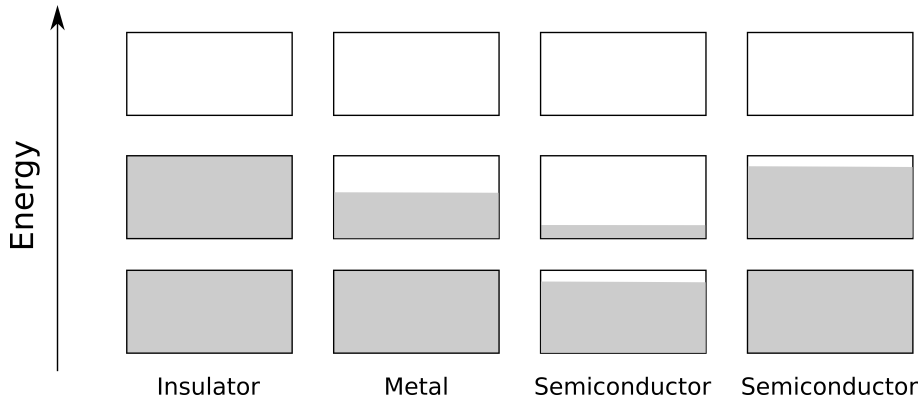

Figure 2.3: Band structure of different materials. The boxes represents energy bands and the gray color represents the occupancy of electrons in the band.

2.2.1 Fermi level and the origin of bands

To understand the origin of the band structure one can start with the free electron Fermi gas model. This model is best utilised for understanding material properties that mainly depends on the kinetics of the conduction electrons and has been successful in explaining things like the Hall effect[14]. We will also find the definition of the Fermi level, a property of the electrons in a solid which can be used to explain charge transfer between adjacent metals.
In this model one treats the conduction electrons as a free gas but still following the Pauli principle. That meaning, all interactions between electrons or electrons and core will be neglected but the condition that no electrons can occupy the same quantum state will be present.
Starting with a one dimensional model of a metal with length L containing only one electron with mass m. One restricts the electron to only move inside the metal by imposing infinite potential barriers at $x = 0$ and $x = L$. Then solving the Schrodinger's equation

$$\hat{\mathcal{H}}\psi = \epsilon_{\mathbf{n}}\psi \quad \text{with} \quad \hat{\mathcal{H}} = \frac{-\hbar}{2m}\frac{d^2}{dx^2}. \tag{2.6}$$

yields wavefunctions

$$\psi_n = \sin\left(\frac{n\pi}{L}x\right) \quad \text{and energies} \quad \epsilon_{\mathbf{n}} = \frac{\hbar^2}{2m}\left(\frac{n\pi}{L}\right)^2. \tag{2.7}$$

The ground state of this metal then contains one conduction electron with the wavefunction $\psi_1 = \sin\left(\frac{\pi}{L}x\right)$ and energy $\epsilon_{\mathbf{1}} = \frac{\hbar^2}{2m}\left(\frac{\pi}{L}\right)^2$.
A metal with N conduction electrons in the ground state is obtained by adding electrons to this system while requiring no electrons in the same quantum state. Remembering that the electrons posses a property called spin, the next occupied state will then be the same as the first electron but with opposite spin. Electron number three will have the wavefunction ψ_2 and energy $\epsilon_{\mathbf{2}}$. When all N electrons are added one finds the Fermi energy $\epsilon_{\mathbf{F}}$ which is defined as the energy of the highest filled level at the ground state (for semi-conductors and insulators the definition of Fermi level can differ).
To go further and understand the band structure and energy gaps illustrated in figure 2.3 one also needs to consider the ion cores of the metals. These are distributed on a periodic lattice with some distance a between them. One now also changes the boundary conditions to be periodic, that meaning $\psi(x)$ should be equal to $\psi(x+L)$. This means that the infinite potential barriers at $x = 0$ and $x = L$ are gone which might be considered weird but we now have a situation where wavefunctions in the middle of the solid is no longer governed by the boundary conditions several million atoms away. With these boundary conditions, solutions will have the form

$$\psi_n(x) = \exp(ikx) \quad \text{with} \quad k = 0, \pm\frac{2\pi}{L}, \pm\frac{4\pi}{L}. \tag{2.8}$$

Recalling that the wavefunctions also can be used to calculate the probability density of finding an electron at x by

$$p(x) = |\psi(x)|^2 \tag{2.9}$$

and the probability of finding an electron between $x = a$ and $x = b$ is

$$\int_a^b |\psi(x)|^2. \tag{2.10}$$

Recalling also the Bragg condition, that at $k = \pm\frac{n\pi}{a}$ travelling waves to the right will be reflected to the left and vice versa [14]. This will result in wavefunctions made up of equal parts travelling to the left and to the right. From these, one can form the standing waves

$$\begin{aligned} \psi(+) &= \exp(i\pi x/a) + \exp(-i\pi x/a) = 2\cos(\pi x/a) \\ \psi(-) &= \exp(i\pi x/a) - \exp(-i\pi x/a) = 2i\sin(\pi x/a). \end{aligned} \tag{2.11}$$

These results in probability density $|\psi(+)|^2 \propto \cos^2(\pi x/a)$ suggesting high probability of finding electrons close to the ion cores and probability density $|\psi(-)|^2 \propto \sin^2(\pi x/a)$ suggesting a higher probability of finding electrons further away from the ion cores. Energetically it's much more favourable for the electrons to be closer to the positive ion cores due to the electromagnetic attraction and the difference here in energy between the $|\psi(+)|^2$ and the $|\psi(-)|^2$ is the origin of the energy gaps observed in materials and the decisive cause of why some materials can be divided into metals, semi-conductors and insulators.

2.2.2 Fermi level equilibration at metal-metal interfaces

For metals there is no apparent energy gap at the Fermi level. This makes the valence electrons very mobile and they can easily travel within the material. This mobility of the electrons can also extend into other metals. When putting two metals into electrical contact one can observe an effect called Fermi level equilibration which means that the Fermi levels of the metals at the interface will equilibrate[5] as illustrated in figure 2.4. The **a)** figure shows energy diagrams of two metals with their conduction bands when there is no electrical contact and the **b)** figure shows the same energy diagrams but with electrical contact between the metals. This equilibration means that electrons resident in one metal will transfer to the other metal and form a dipole at the interface.

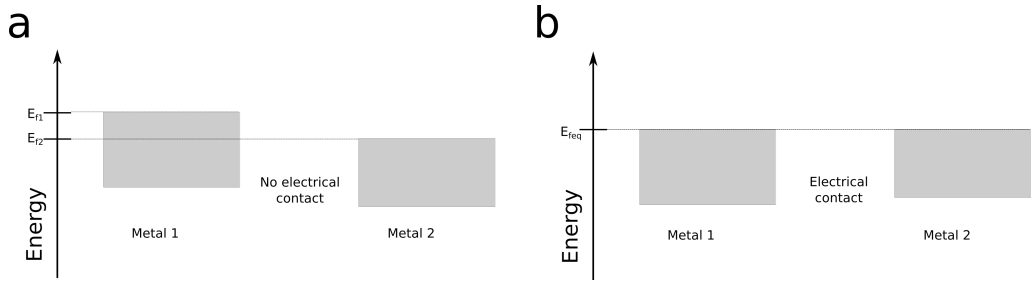

Figure 2.4: **a)** Energy diagram of the conduction band of two metals with no electrical contact. **b)** Energy diagram of two metals with electrical contact and their Fermi level equilibrated.

2.2.3 Metal-insulator-metal structures

Metal-insulator-metal structures consists of two metals separated by an insulator. This creates barrier hindering Fermi level equilibration, as illustrated in 2.5 where the metals are separated by an potential barrier. For the electrons to equilibrate the Fermi level they first need to overcome the potential barrier. The height of the barrier are either determined by the work functions of the metals (the energy needed to remove an electron from the material) or the energy of the conduction band of the insulator[15]. In the figure, the potential barrier is determined by the work functions W_1 and W_2 of two different metals which would be the case if the barrier is vacuum. With an insulator, the barrier could be lowered if the energy needed to reach the conduction band in the insulator is lower than the work functions.
Another way for electrons to overcome the barrier is by quantum tunnelling, the width of the barrier is then detrimental and the probability is decreasing exponentially with the width of an rectangular potential barrier[16].

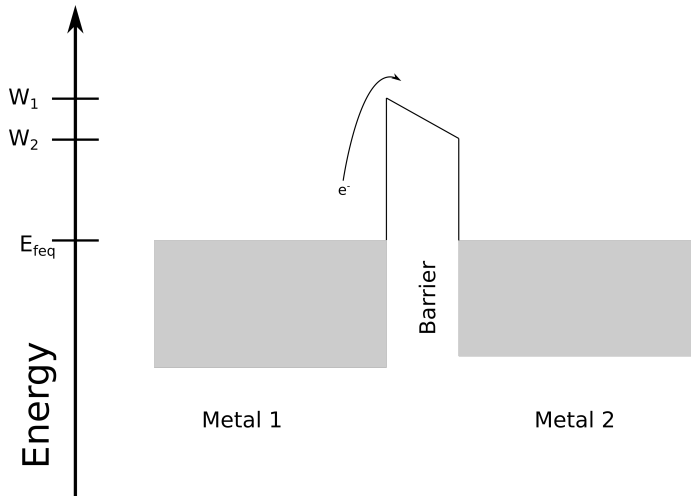

Figure 2.5: Fermi level equilibration of two metals separated by an insulator. To obtain Fermi level equilibration, the electrons must overcome the potential barrier or tunnel through it.

2.3 Nanofabrication: Hole-Mask Colloidal Lithography

Fabrication of nanostructures on a surface substrate can roughly be divided into two different methods. 1. top-down, where a bulk material is cut and milled down into desired shaped nanostructures and 2. bottom-up where the nanostructures are built from the ground up using chemical and physical properties of atoms and molecules to self-assembly into desired nanostructures.
Hole-Mask Colloidal Lithography is a bottom-up technique developed here at Chalmers University of Technology [17] where a substrate is covered with a mask containing nano sized holes. In these holes, nanoparticles can be built in a variety of configurations using different deposing techniques of materials over the substrate surface.

When the nanoparticles in the holes has the desired shape, one simply removes the mask leaving the surface with an array of the fabricated nanoparticles. The general fabrication steps are summarised in figure 2.6 but for a more detailed description on how to vary the steps to achieve different nanoparticles I refer you to literature such as [17] and [18].

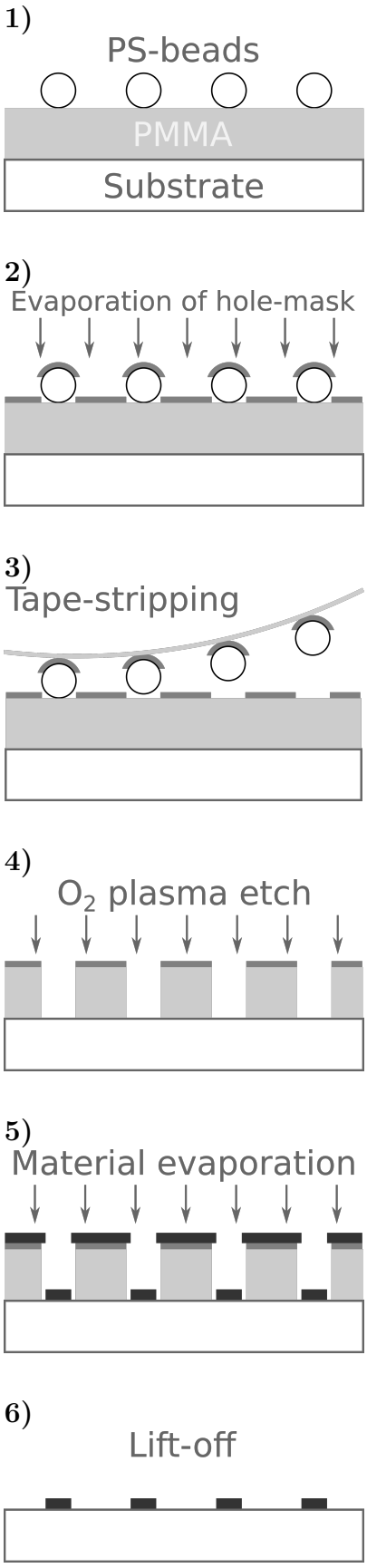

Figure 2.6:

1. PMMA is first spincoated on a substrate. Then, a suspension of PS-beads is added to the substrate. The beads will adsorb onto the PMMA film.
2. With the PS-bead adsorbed, a thin film of either Au or Cr is deposited on the substrate.
3. Taping the surface and then stripping it of will remove the PS-beads. Leaving nanoholes in the deposited gold film.
4. Exposing the surface to oxygen plasma will etch holes through the PMMA.
5. Building the nanoparticles by deposing material through the holes. This can be done with different methods, such as atomic layer deposition where a thin layer of a material is grown on the substrate or a thermal evaporator where the deposition material is heated up until it evaporates, then condensing on the substrate.
6. In the final step, the mask is removed using acetone leaving the nanostructures on the substrate.

2.4 Experimental techniques

2.4.1 XPS - X-ray Photoelectron Spectroscopy

X-ray photoelectron spectroscopy (XPS) is a surface characterisation method utilising the emission of electrons from a surface when irradiated with high energy photons. By measuring and analysing the kinetic energy of these emitted electrons one can gain information about the composition of the surface and the elements chemical and electronic state.
The technique is based on the photoelectric effect, in which the energy of photons is absorbed by the electrons in an atom. If the energy of the photon is high enough the electron can escape from the atom. The kinetic energy the electron will posses is then the energy of the photon $h\nu$ minus the binding energy E_{bin}

$$E_{kin} = h\nu - E_{bin}. \tag{2.12}$$

The binding energy of the electron depends on the type of atom and the shell it's in and the energy of the photon depends on what x-ray source it comes from. If one knows the energy of the photon and one can measure the kinetic energy of the electron one can then calculate the binding energy by

$$E_{bin} = h\nu - E_{kin}. \tag{2.13}$$

Matching this energy to known values of binding energy of elements one can draw conclusion about what element, what chemical state and if its electronic state is affected.
In reality when doing XPS measurements one typically also need to consider some artefacts and limitations of the method. Background signal and charging of the sample will be explained shortly here but for other things such as Auger peaks and plasmon excitation I refer to literature as [7].

Background signal

In XPS spectras one can typically see some kind of background or "shoulders" to the left of all peaks as illustrated in figure 2.7. These occur when electrons are excited below surface level and has to travel through the sample before reaching the analyser. While travelling through the sample the electrons will lose some of their energy and this give rise to the higher signal to the left of the peak.
When analysing spectras one has to compensate for these shoulders. The common way of doing this is subtracting a Shirley background which can be related to a certain cross-section function or probability function describing the energy loss of the electrons[20].

Charging

Due to the loss of electrons when exciting photolecrons the sample will build up some positive charge. This will shift all peaks in the spectrum to higher energies by the same amount[7]. Depending on if the sample is conducting or not, this shift

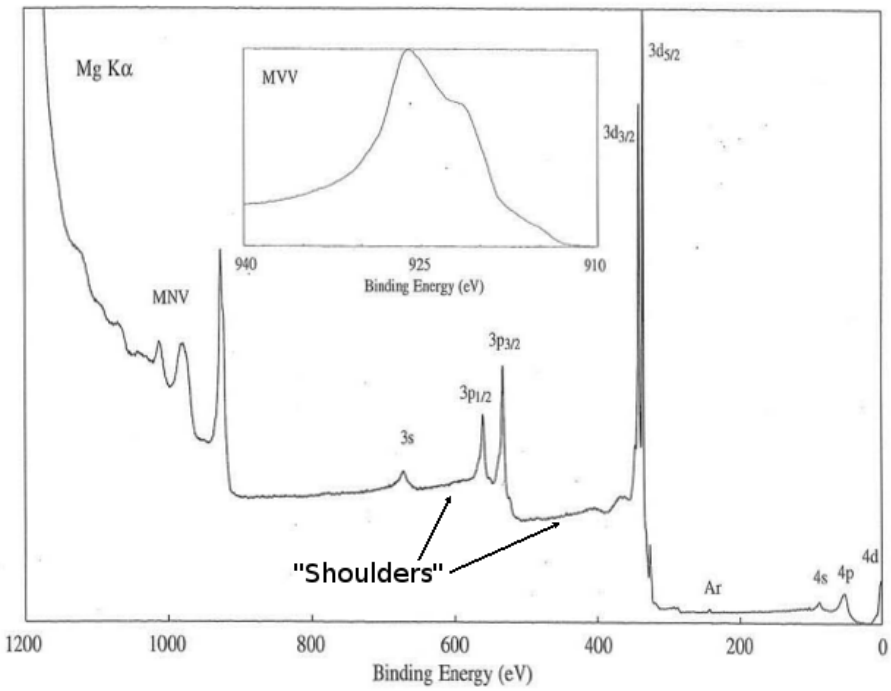

Figure 2.7: XPS spectra of a Pd surface. The higher intensity to the left of each peak (the "shoulders") occurs because of electrons travelling through the sample. Image taken from *Handbook of X-ray Photoelectron Spectroscopy*[19].

can be almost insignificant or several eV. If the shift is large one can typically use a low energy electron gun to provide more electrons to the sample and reduce the charging effect. In the analysis one also typically make use of a reference peak with a known binding energy and shifts all peaks the same amount to position this peak at its known binding energy.

2.4.2 QMS - Quadrupole mass spectrometry

A quadrupole mass spectrometer can be used to measure chemical species in gases. It works by ionising incoming gas species and then with an variable electric quadrupole field it filters out species with high and low mass to charge ratios. Leaving only a narrow band of species with certain mass to charge ratio to pass through[21]. By measuring the ion current produced by these, one can get information of how much of a certain species exists in the incoming gas.

2.4.3 SEM - Scanning Electron Microscope

Scanning electron microscopy is a commonly used imaging technique of surfaces. With a resolution of down to less than a nanometer [22] one can obtain images with well resolved nanostructures. It works by scanning the sample surface with a focused electron beam. The electrons will interact with the surface in several different ways and by measuring and analysing these interactions one can build up an image of the surface.

The most commonly used interaction is the secondary electrons which are electrons knocked out from atoms close to the surface[22]. These electrons have typically less energy than 50 eV and carries information of both the sample chemistry and the topology of the sample. The low energy of these electrons restricts how far in the sample they can travel and they are typically emitted less than 10 nm from the surface.
In reality when doing SEM imaging there are a couple of parameters one has to consider to obtain a good image. One is the accelerating voltage of the electron beam which determines what energy the electrons in the beam will have when colliding with the sample. A too low energetic beam will not excite any secondary electrons and a too high energetic beam will travel to far into the sample and excite electrons far from the surface and the focusing point. An other thing is the width of the electron beam, a high energetic beam will be more focused, because there is not that much time for the electrons to feel the electromagnetic repulsion. The beam current also effects the width of the beam. A too high current will widen the beam and a too low current will not excite enough electrons to obtain enough signal.

3
Methods

3.1 Modifications of the flow reactor

With inspiration from previous work by Hans Fredriksson et. al [8] two modifications of the existing flow reactor were done. First the sample holder of the existing flow reactor was replaced by a sample holder of glass. This sample holder encapsulates the entire sample, forcing the reacting gases to pass by close to the sample before going into the mass spectrometer. An image of it can be seen in figure 3.1 **b** and will be referred to as the "pocket reactor", the old setup will be referred to as the "sniffer" and can be seen in figure 3.1 **a**. This encapsulation of the sample should reduce the dilution of the catalysis products as illustrated in figure 1.2 which would increase the too low signal produced by the catalyst product in the mass spectrometer.
The second modification was an addition of an extra mass flow controller at the outlet of the pocket reactor to create a variable exhaust. This modification is illustrated in figure 3.2 and should allow for either regulating or measuring the flow rate through the pocket reactor. This was though not tested in detail, the variable exhaust was kept closed at all the following measurements.

3.1.1 Verifying the new setup

To verify that these modification improves the sensitivity an experiment with carbon monoxide oxidation was performed. First, the background activity of both the sniffer and the pocket reactor was obtained. This was done by first heating up the reactors to 222 C° with a flow of 200 ml/min Argon. Then CO and O_2 was introduced in to the reactor. The total flow rate was kept constant at 200 ml/min and the flow rate of CO was kept constant at 4 ml/min. In steps, the flow rate of O_2 and Ar was then changed to obtain different CO to O_2 ratios. Each step lasted for 30 min except for the first which lasted for 60 min with the purpose of reaching a steady readout from the mass spectrometer. The order of the steps and the different ratios used was 3, 5, 10, 30, 50 and 90 % vol CO.
Same experiment was then repeated with a test sample, both in the pocket reactor and in the sniffer. The sample consisted of core shell nanoparticles, the core was a gold disk covered in a 5 nm Al_2O_3 shell covered with small platinum nanoparticles of roughly 5 nm diameter.
The analysis consisted of comparing the background activity of the two setups by comparing the ion currents of the CO_2 produced in the empty reactors. The activity from the reactors with the samples inserted was then compared in the same way. Finally the activity of only the samples was compared by subtracting the ion current

produced from the empty reactors from the ion current produced when the sample was inserted.

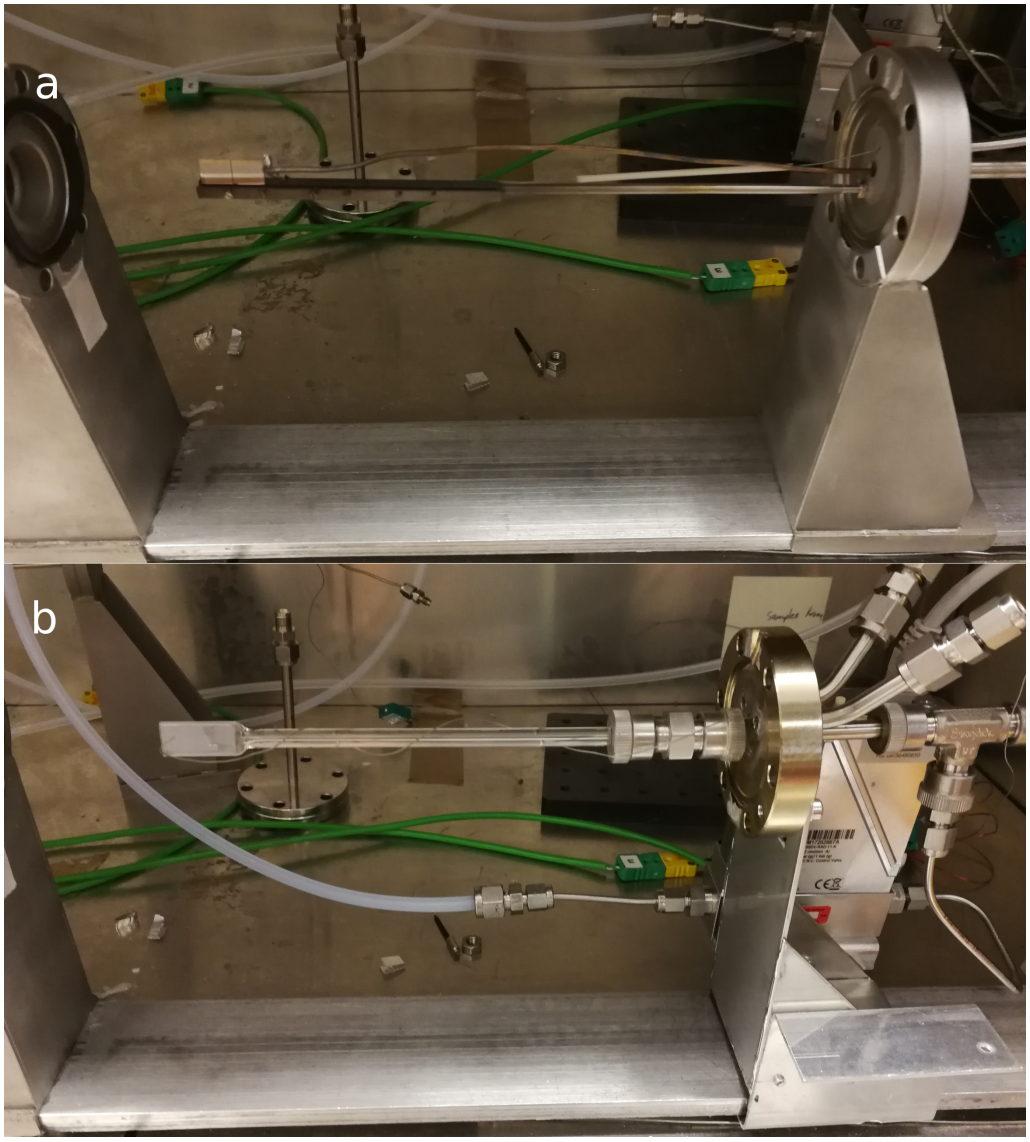

Figure 3.1: a) The old ”sniffer” setup where the collection of catalyst products is done by the tube close to the sample. **b)** The new pocket reactor which encapsulates the sample, reducing dilution of the catalyst products.

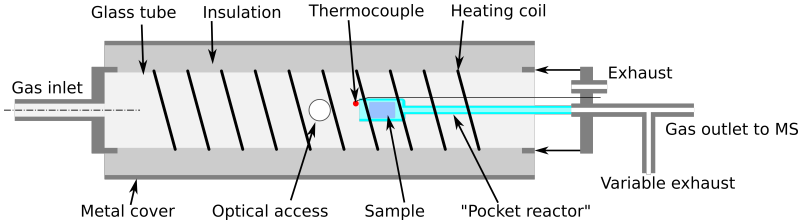

Figure 3.2: A schematic drawing of the flow reactor with the implemented glass pocket reactor and the variable exhaust.

3.2 Fabrication of core shell nanoparticles

The fabrication of the core shell nanoparticle samples was done in the MC2 Nanofabrication Laboratory, at Chalmers University of Technology which is a cleanroom environment with ISO 14644-1 certification, all samples was fabricated by Arturo Susarrey-Arce and Christopher Tiburski. Two sets of samples, one set with a silicon substrate and one set with a fused silica substrate. The silicon is a semiconductor and should help prevent charging in XPS and SEM measurements. The fused silica is transparent and allows for easy collection of the optical spectra of the nanoparticles. The fabrication followed these steps:

1. Cleaning the substrates by putting them in an acetone bath during sonication for 1 min, then rinsing in isopropanol followed by blow drying with N_2.
2. Spin coating a primer, HMDS at 3000 rpm with an initial acceleration of 2000 rpm/min for a total of 30 s.
3. Baking the samples on a hotplate at 115 ° for 2 min to evaporate residual solvents.
4. Spin coating PMMA (2 wt % diluted in anisole, molecular weight M_w = 950 000 from MicroChem Corporation) at 7500 rpm with an initial acceleration of 2000 rpm/min for a total 60 s.
5. Baking the samples on a hotplate at 150 ° for 5 min to evaporate residual solvents.
6. Exposing the samples to O_2 plasma for 5 second at a pressure of 250 mTorr, RF power 50 W and an oxygen flow of 10 sccm. This makes the PMMA surface more hydrophilic which facilitates interaction with particles dissolved in aqueous solutions.
7. Drop coating the substrates with PDDA (M_w = 100 000 – 2000 000 from Sigma-Aldrich), leaving it on for 30 s. PDDA is a positively charged polyelectrolyte that forms a positively charged monolayer on the substrates.
8. Rinsing in water followed by blow drying with N_2.
9. Drop coating the substrates with a colloidal suspension of polystyren beads (PS-beads). These PS-beads are negatively charged and adsorbs to the positively charged substrate, forming a sparse monolayer of Polystyrene. The repulsion between the PS-beads prevents clustering of the beads.
10. Blow drying with N_2.
11. Evaporating a 20 nm thin gold layer using electron-beam physical vapour deposition in a Lesker PVD 225. With the rate 1.5 Å/s at a pressure of 5e-7 Torr.
12. Tape stripping the substrates to remove the PS-beads and creating the hole mask.
13. Exposing the samples to O_2 plasma conditions as above but for 1 min and 25 s. This etches holes down to the silicon/fused silica surfaces.
14. Again evaporating a 20 nm gold, same conditions as in previous step. This creates the core of the nanoparticles.
15. With atomic layer deposition, different thicknesses of Al_2O_3 films was deposited on the samples. This was done using atomic layer deposition (ALD), varying the number of cycles between 2-12 cycles for the different samples.

16. Putting the samples in a water bath for 2 min followed by blow drying with N_2. Then tape stripping to remove Al_2O_3 on the top of the mask to open up the holes in the mask, allowing for depositing more material through the holes.
17. Evaporating a 2 nm thin Pd/Pt film using electron-beam physical vapour deposition in a Lesker machine.
18. Lifting off the mask by putting the samples in sonication baths of mr-Rem 700 (Microresist Technology GmbH) for 1 min, then isopropanol for 1 min and finally acetone for 1 min.
19. Blow drying with N_2
20. Thermally annealing the samples for 6 h at 220°C in a 100 ml/min flow of 4 % vol H_2 diluted in 96 % vol Ar. The purpose of this step is to thermally stabilise the nanoparticles. In this steps, the thin layer of Pd or Pt should form nanoparticles with a diameter of roughly 3-4 nm.

3.2.1 Control samples

To ensure that the gold core of the nanoparticles actually are participating in the catalysis, two sets of control samples was also fabricated. These were fabricated on fused silica substrates and followed the same fabrication steps as the core shells, except for deposition of the gold core. This step was simply skipped and should result in samples with Al_2O_3 films of different thicknesses with Pd and Pt particles on the top.
Two samples with Al_2O_3 cores was also fabricated, one with Pd and one with Pt on top. These followed the same recipe as the other samples except that instead of evaporating a gold core, Al_2O_3 was evaporated. No deposition of Al_2O_3 using the ALD was performed on these samples.

3.3 Sample characterisation

3.3.1 XPS measurements

To ensure that the fabrication succeeded in terms of that the existing species on the samples are expected and wanted XPS measurements was performed. To get an overview of the chemical species present on the samples spectras between 0 and 1193 eV was obtained.
From these spectras a qualitative analysis was performed by assigning the peaks in the spectras to known binding energies of chemical species. Then, to confirm that the samples with more cycles of Al_2O_3 actually had a thicker shell covering the gold core, the area underneath the gold peaks was compared with the area aluminium peaks. With a thicker shell, less electrons from the core should get excited and the Al_2O_3 to Au ratio should increase.
Then, to be able to resolve oxidation states of Pd and Pt, high resolution scans were performed including only the energy regions of Pd3d and the Pt4f peaks respectively. This was also done for C1s peak with the purpose of using this peak as reference peak, compensating for charging.

For the high resolution peaks a deconvolution of the peaks was performed. First a Shirley background was subtracted, then Voigt functions which is a convolution of a Gauss function and a Lorentz function was fitted to the data. For the Pd3d and the Pt4f peak, six Voigt functions was used representing pure metal, the oxides PdO/PtO and PdO_2/PtO_2 and the spin orbit splitting of each peak. For the C1s peak, three Voigt functions was used representing C−C, C−O−C and O−C=O. The software used for the analysis was *Jupyter Notebook* together with the python package *ttlab*[1].

3.3.2 SEM imaging

To control that the fabricated core shell samples actually had the expected and desirable shapes, SEM images was taken of the samples. To help prevent charging, the samples with silicon substrate was used.

3.4 Measuring CO oxidation

To investigate how the shell thickness of the core shell samples affects the catalytic activity of CO oxidation, experiments was performed in the pocket reactor. Same experiments was performed for all samples and consisted of flowing CO and O_2 in to the reactor, increasing the temperature and measuring the products with the mass spectrometer. Using the ion current of CO_2 and the sample temperature, the activation energy was calculated.

3.4.1 Reaction conditions

To achieve the same initial reaction conditions for each sample a pre-treatment of the samples was performed. This pre-treatment consisted of three steps,

1. heating up the sample to 222 C° in 100 % Argon, 100 ml/min flow rate, 10 C°/min,
2. keeping the sample at 222 C°, 97 vol % Argon and 3 % H_2, 100 ml/min for one hour,
3. lowering the temperature to 196 C° in 100 % Argon, 100 ml/min flow rate and keeping it for one hour.

The H_2 here works as a reducing agent and should get the sample to roughly the same conditions before each experiment. Two different ratios of CO and O_2 was then investigated. First, a ratio of 50 % vol CO and 50 % vol O_2 with a flow rate of 2 ml/min for the CO, with argon as a carrier gas to reach 100 ml/min. After introducing this mixture an equilibration time of 1.5-2 h at 196 C° was initiating the experiment. This was done with purpose of reaching a stable readout from the mass spectrometer. After this, the temperature was increased by 4-5 °C four times with a temperature ramping of 5°C/min. Each temperature increase was followed by an equilibration of 30 or 15 min depending on if it was a Pd or Pt sample. When these steps had ended a pre-treatment was again started. Then the second ratio which was 5 % vol CO and 95 % vol O_2 with a flow rate of 2 ml/min for the CO, again with argon as a carrying gas to reach a total flow rate of 100 ml/min. This

experiment also started with an equilibration time of 1.5-2h but at 188 °C. The same temperature ramping was then performed, with the same equilibration time for each step.

4

Results

4.1 Higher signal with the pocket reactor

The background activity of the pocket reactor and the sniffer is roughly the same. This can be seen in figure 4.1a where the ion current produced by CO_2 is plotted. The dashed vertical lines shows where the ratio of CO and O_2 is changing and the vol percentage of CO can be found underneath the graphs. The activity is highest at the 3 % CO which hints that the reaction is occurring at some surface. Otherwise, the activity would be highest at roughly 66 % CO suggested from the balanced reaction equation

$$2\,CO + O_2 \longrightarrow 2\,CO_2. \tag{4.1}$$

In figure 4.1b, the same experiment as in the top figure was performed but with the sample in the reactor. One can see that the signal is much higher for the pocket reactor compared to the sniffer and in figure 4.1c one can see the ion current with the background subtracted. One can see that the pocket reactor signal is roughly two orders of magnitude higher.

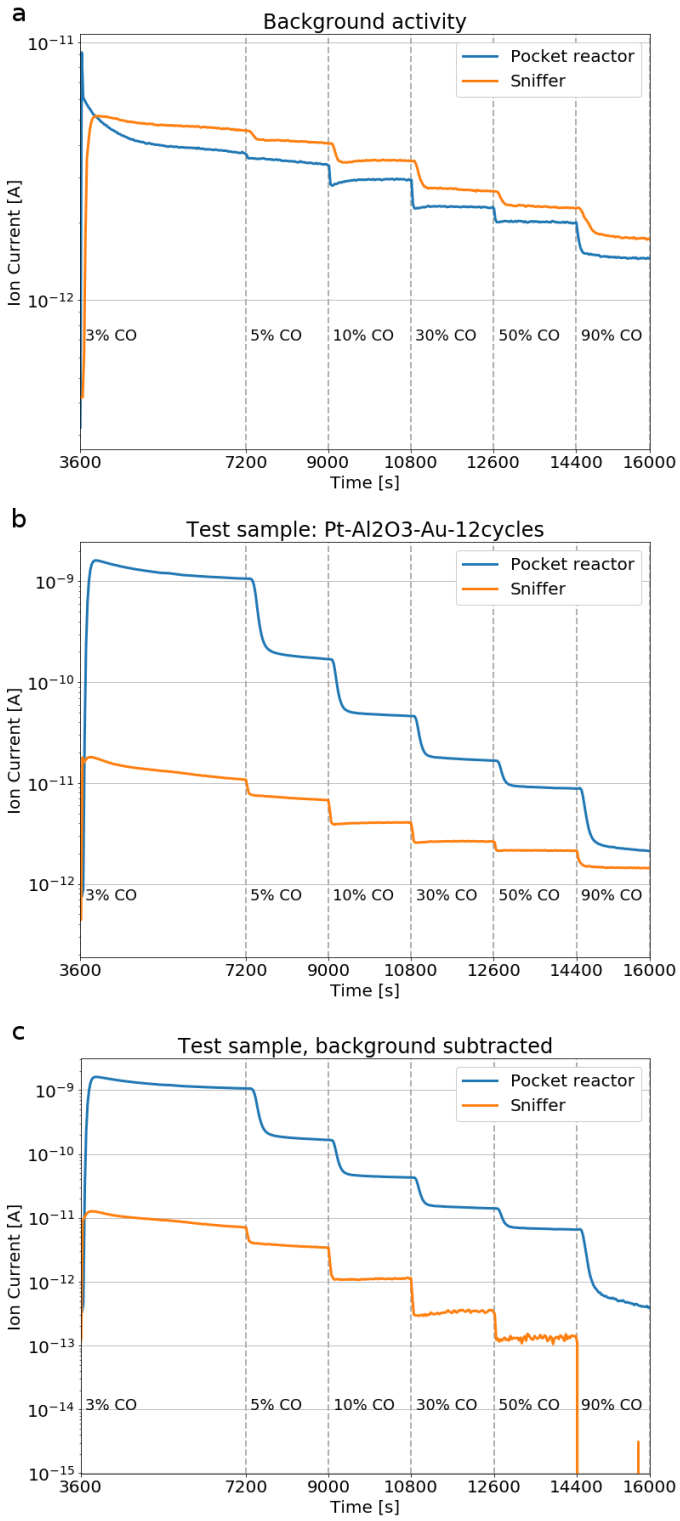

Figure 4.1: The ion current produced by CO_2 for different vol concentrations of CO and O_2. a) Without any sample in the reactor. b) With a test sample containing core shell particles with a gold core, 12 ALD cycles of Al_2O_3 and Pd catalysts. c) The background subtracted from the signal with the sample.

4.2 Fabricated samples

A total of 40 samples was fabricated, half of them had Platinum as catalyst and the other half had Palladium. The shell thicknesses obtained varied between 2 and 12 cycles of ALD. This should correspond to Al_2O_3 thicknesses between 1 and 5 nm. To simplify describing the samples from here on, abbreviations will be used. For example, a sample which contains nanoparticles with Pd catalysts, x ALD cycles of Al_2O_3 and a gold core will have the abbreviation "Pd-Al_2O_3-Au-xcycles". The controls which don't have a gold core will have the abbreviation "Pd-Al_2O_3-xcycles" and the samples which do not have any Al_2O_3 will be referred to as "Pd-Au", "Pd" and "Au" which corresponds respectively to a sample containing nanoparticles with a gold core with Pd catalysts on a top, Pd catalysts directly on the substrate and a sample with only gold cores.

4.2.1 XPS data confirms the varying thickness of the shells

In figure 4.2 the whole spectrum from the XPS measurements can be seen for the samples containing Pd catalysts on gold cores. The position of the C1s peak has been used as a reference peak and the whole spectrum has been shifted to have the C1s peak at 284.8 eV. One should also mention that the O1s peak has been truncated for the purpose of fitting all spectras in the same figure and keeping the possibility of resolving smaller peaks.
One can see that the samples has the expected elements. Looking at the Au4f peaks and comparing them with the Al2p peaks one can see that when samples has more cycles of Al2O3, the Au4f peak decreases and at the same time the Al2p peak increases. This can also be seen in figure 4.3 where the area underneath the Al2p peak is divided by the area underneath the Au4f peak and plotted against shell thickness.

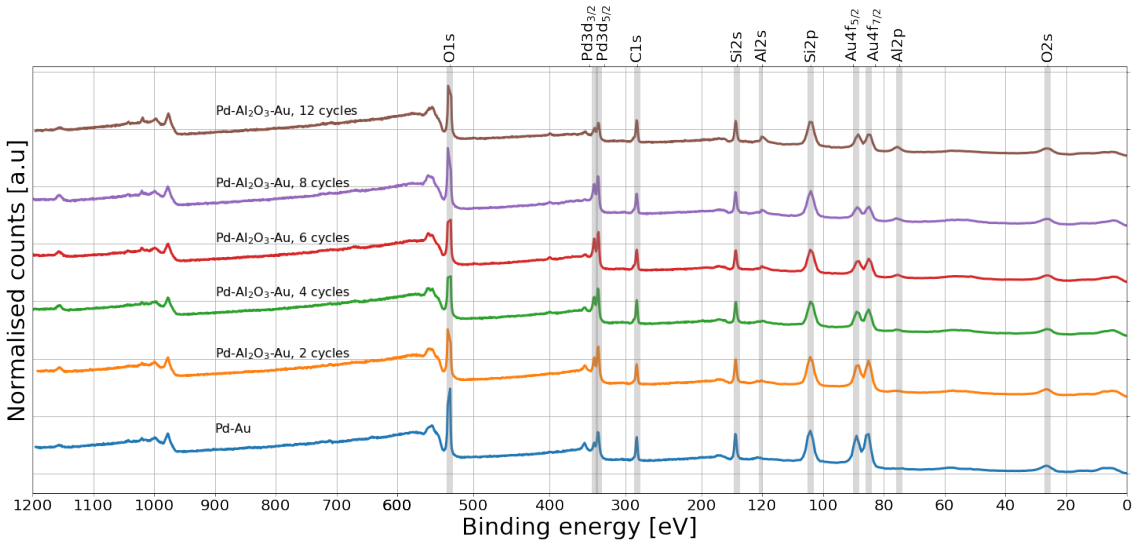

Figure 4.2: XPS measurements for samples containing core shell particles with different thickness of Al_2O_3. The O1s peak has been truncated with the purpose of fitting all spectras in the figure.

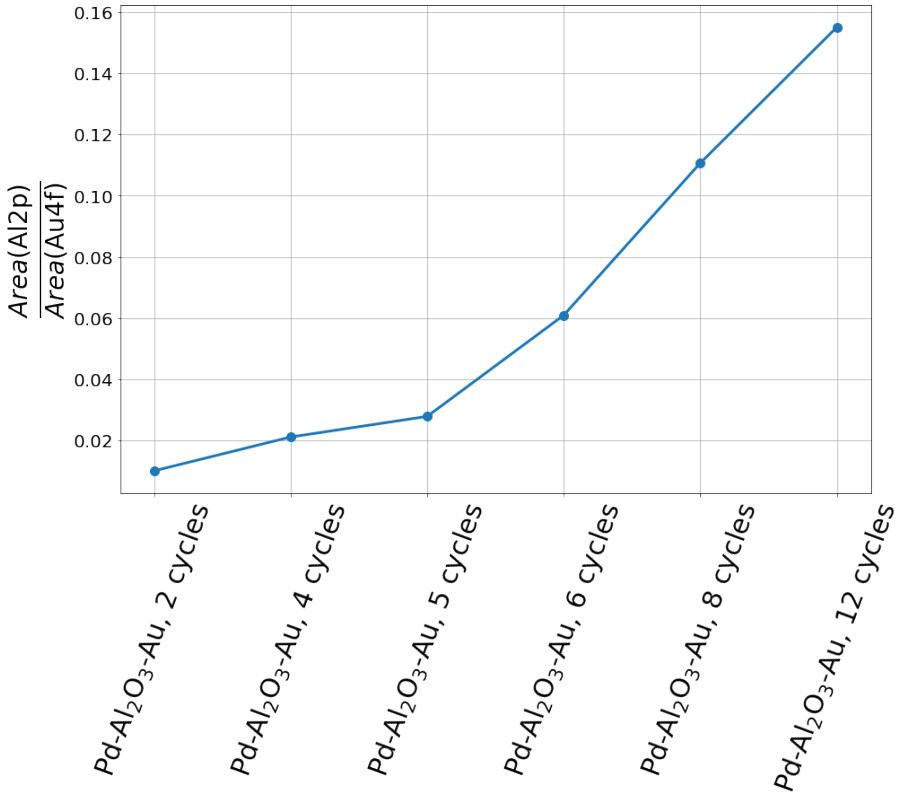

Figure 4.3: The ratio of the area underneath the Al2p peak and the area underneath the Au4f peak. The monotonic increases indicates that the Al_2O_3 shell thickness increases with the number of ALD cycles.

4.2.2 Pd oxides and shell thickness

From the high resolution XPS measurement of the palladium Pd3d peak one can see two well separated peaks. This is shown in figure 4.4, where the XPS signal from the Pd-Al_2O_3-Au-6cycles sample is plotted. According to XPS table [19] these are the spin-orbit separated $Pd3d_{3/2}$ (low energy) and $Pd3d_{5/2}$ (high energy) peaks.

Note that a Shirley background has been subtracted and six Voigt functions has been fitted to the measured data. The width, height and position of these agrees well with literature values of Pd, PdO and PdO_2, see the table in figure 4.5. The corresponding species to each Voigt function can also be found above the graph in figure 4.4.

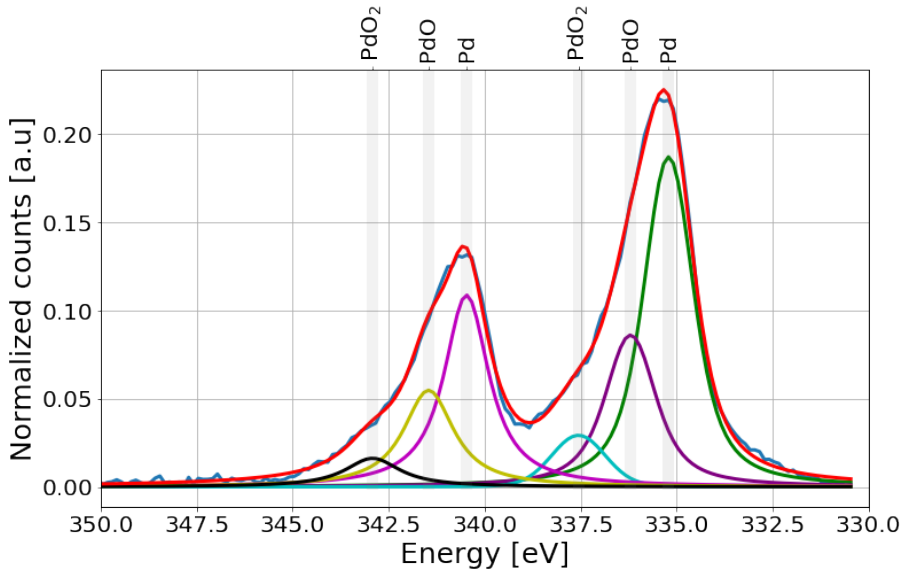

Figure 4.4: The palladium Pd3d peak acquired from the sample with 6 cycles of Al_2O_3 with six Voigt functions fitted to the data. The corresponding Pd species can be found above the figure.

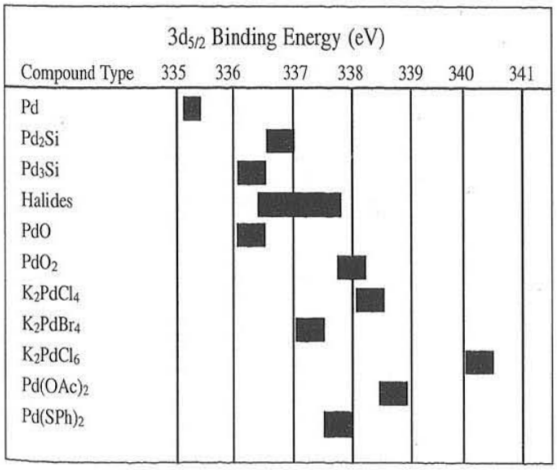

Figure 4.5: Binding energies of Pd compounds. Table copied from *Handbook of X-ray Photoelectron Spectroscopy*[19].

More Pd3d peaks from other samples can be found to the left in figure 4.6. Note here the shape of the peaks, a sample with more cycles of Al_2O_3 seems to have a bump at roughly 338 eV. This could be a result of more PdO_2 present on these samples. A quantitative analysis by fitting Voigt functions was though not possible due to the much higher noise, especially in the samples with 8 and 12 cycles of Al_2O_3.

To the right in figure 4.6 one can see the Pt4f peaks from the platinum samples. Compared to the Pd samples these seems much more uniform, the thickness of the Al_2O_3 sample does not seem to have a any impact on oxides forming on the Pt.

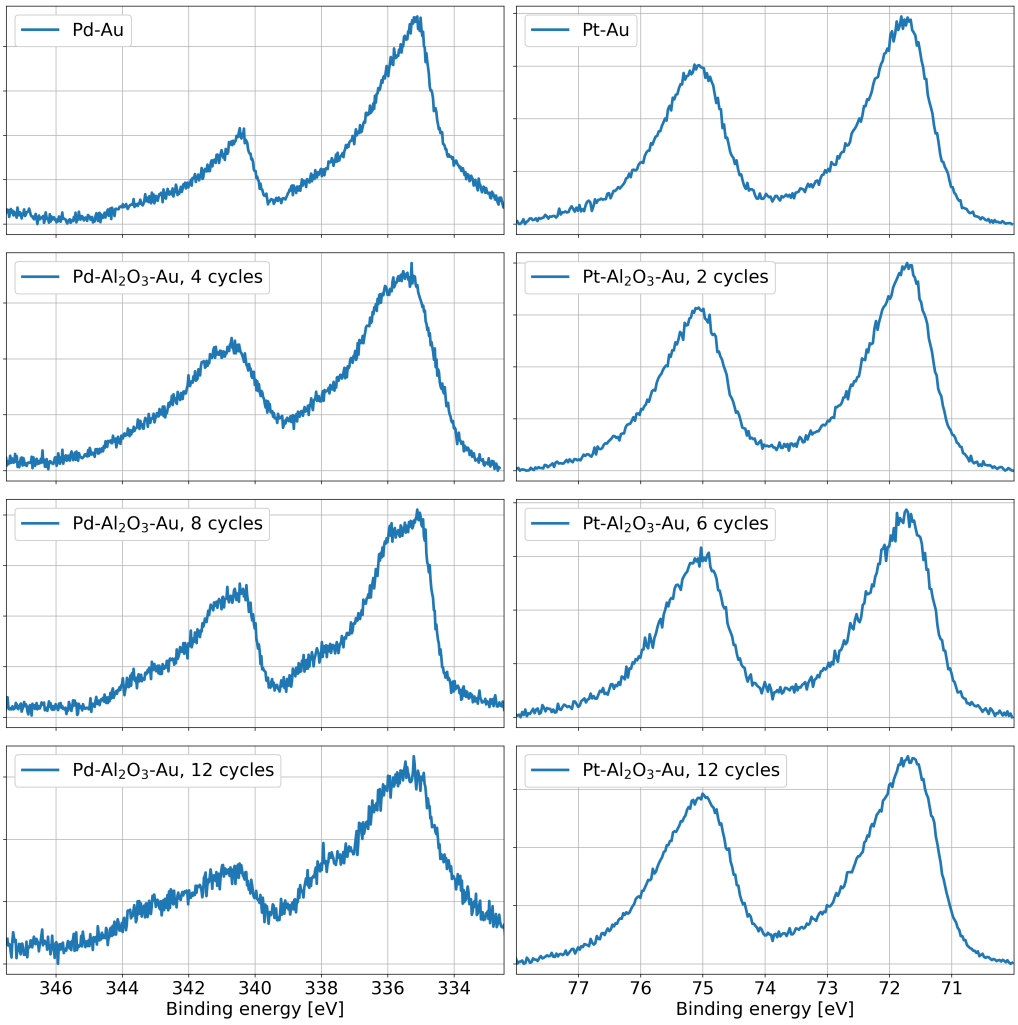

Figure 4.6: Pd3d peaks to the left and Pt4f peaks to the right measured in XPS. The number of Al_2O_3 cycles on the samples increases when going down in the figures.

4.2.3 SEM images, possible alloying between gold and palladium

The SEM images that was acquired can be seen in figure 4.7. These was taken at an angle to get the 3-dimensional view. Note the small particles on top and around the samples with 4 or more cycles of Al2O3. These are the Pd catalyst particles formed during the annealing. On the sample Pd-Au and Pd-Al_2O_3-Au-2cycles one can't resolve any particles on top. This could mean that during the annealing, the Pd and the Au core has formed an alloy. For the Pd-Al_2O_3-Au-2cycles sample this could also indicate that the core is not fully covered in Al_2O_3, which should otherwise prevent alloying.

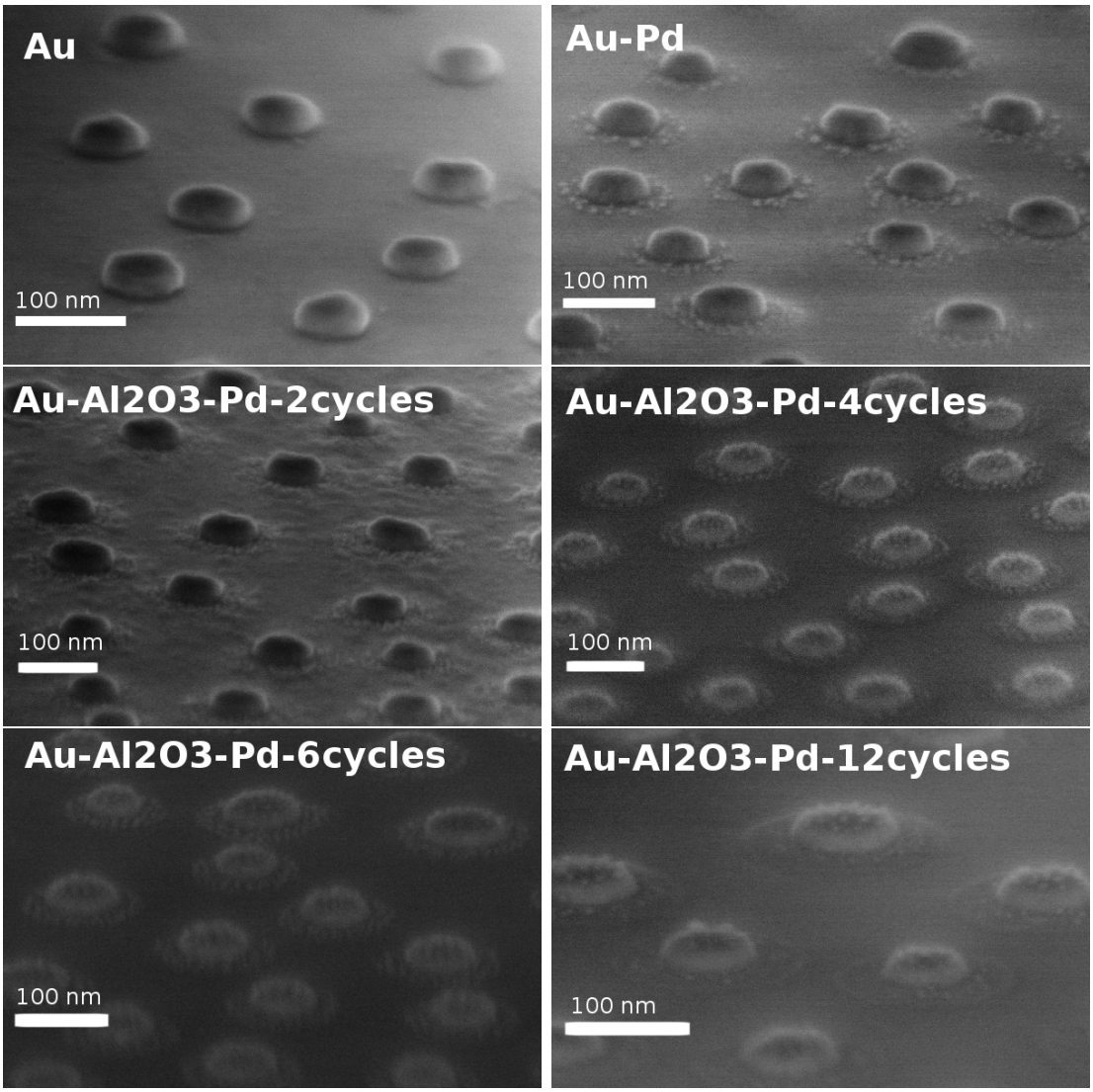

Figure 4.7: SEM images of the Pd samples. Pd on top of the samples can be distinguished on the samples with 4 cycles of Al_2O_3 or more.

4.3 CO oxidation, shell thickness effect on activation energy

The calculated activation energy from the experiments with oxidation of carbon monoxide can be seen in figure 4.8-4.10, the error bars in these shows the standard deviation of data points from the fitted straight line.
In figure 4.8 one can find the activation energy for the samples with a gold core and the reaction condition 5 % vol CO. To the left one can see the samples having Pd as a catalyst and to the right the samples having Pt. Notice that the activation energy here seems to follow the same trend for both Pd and Pt though shifted to a higher energy for the Pd samples. Both the Pd and Pt samples seems to reach a plateau after 6-8 cycles of Al_2O_3 where the difference in activation energy does not differ as much anymore, and for the sample with the Al_2O_3 core one can see a decrease

in activation energy for both catalysts. These similar trends could be an indication that the same reaction mechanism is occurring on both samples and is affected in the same way.

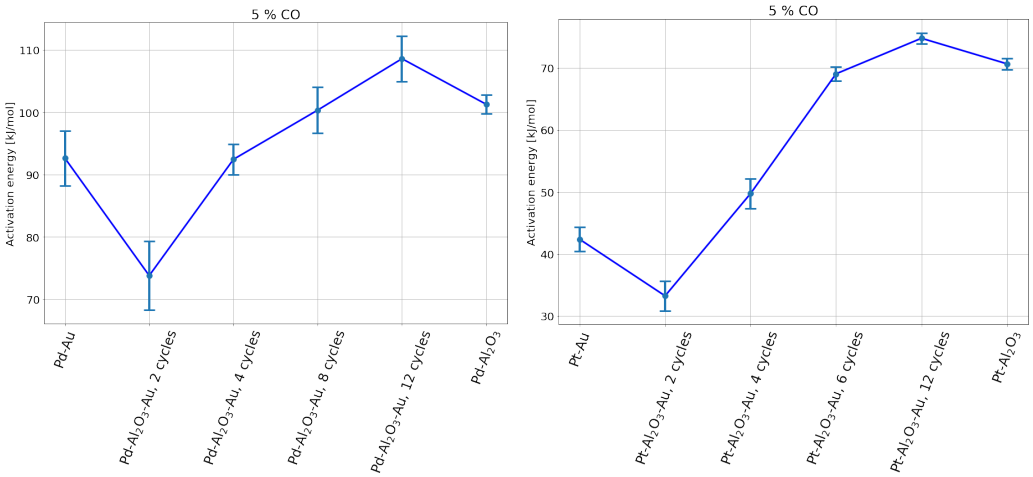

Figure 4.8: Activation energy calculated from the experiment with 5 % CO. In the left figure for the Pd core shell samples and in the right for the Pt core shell samples. The error bar shows the standard deviation from the a straight line in the Arrhenius plot.

Moving on to the activation energy with 50 % vol CO, shown in figure 4.9. One can see that the trend for the Pd and Pt samples are totally different. The Pt samples has a similar trend as the 5 % vol CO except for the 2 cycle sample which is here higher than the Pt-Au sample. But the activation energy for the Pd samples does not follow the same trend at all. The huge jump between 2 and 4 cycles is interesting and hints that something is changing drastically in the reaction mechanism.

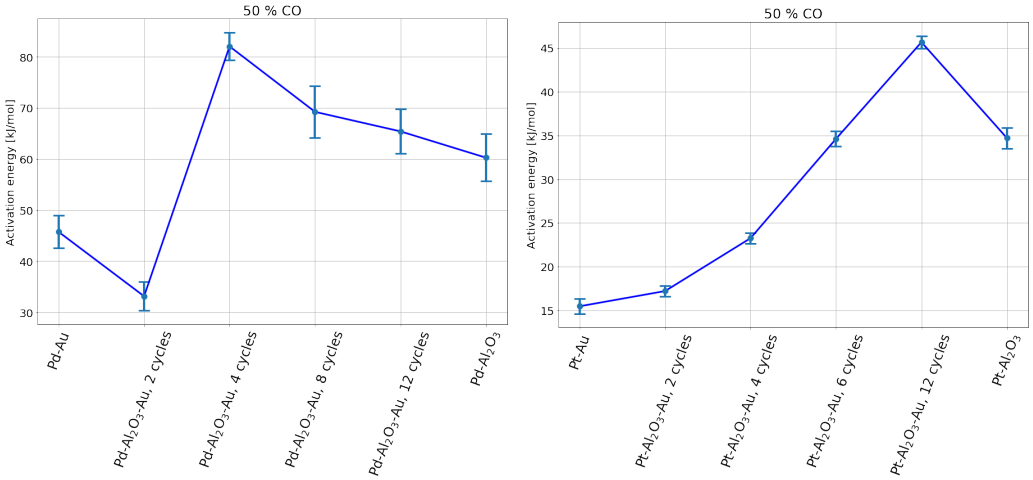

Figure 4.9: Activation energy calculated from the experiment with 50 % CO. In the left figure for the Pd core shell samples and in the right for the Pt core shell samples. The error bar shows the standard deviation from the a straight line in the Arrhenius plot.

The control sample, the ones without a gold core have again a different activation energy trend than the samples with the gold core, this can be seen in figure 4.10. Interestingly here, is that the trends look similar for both the 5 % vol CO and the 50 % vol CO. This is consistent for both the Pd and the Pt samples. Among the Pt samples there is one activation energy that stands out, namely the 4 cycle sample. This one has a much larger error bar than the others which mean that it deviates more from the Arrhenius equation. This could be a coincident, but the fact that the 50 % vol CO and the 5 % vol CO measurement was done on two different days reduces the chances of this being a coincidence of experiment factors. But could still be something wrong with the sample.

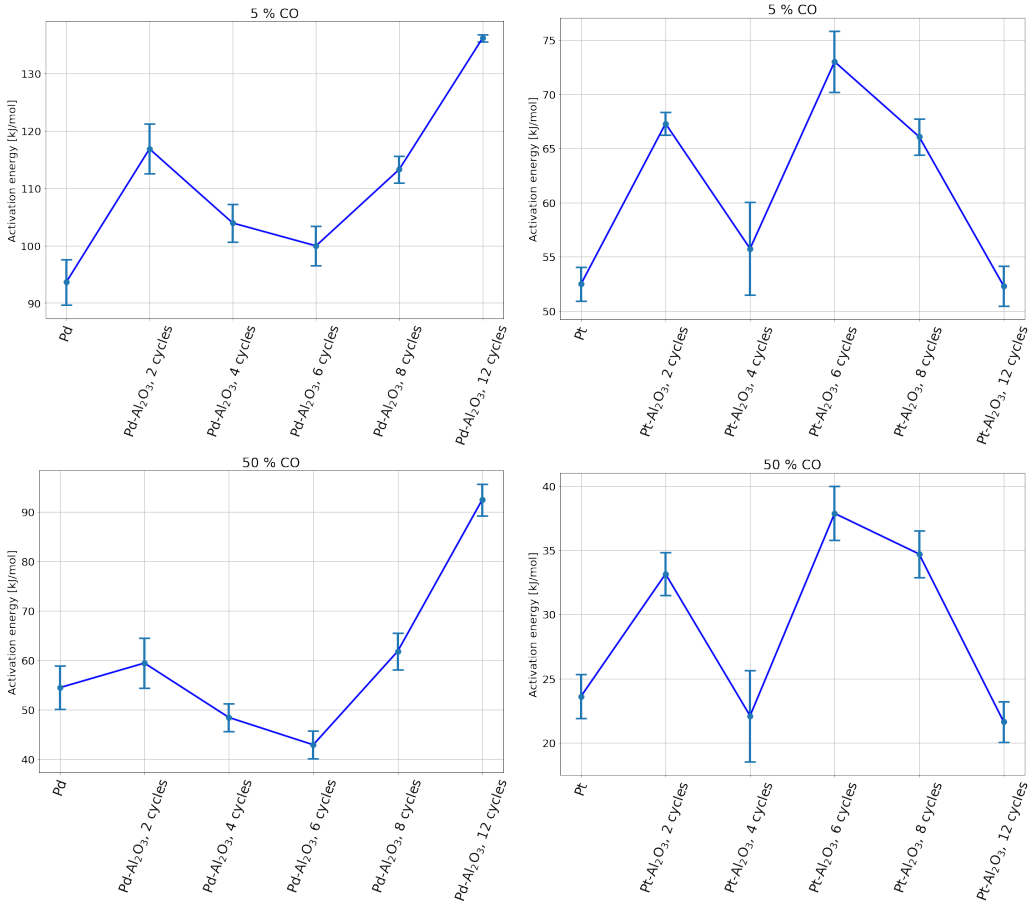

Figure 4.10: Activation energy calculated from the experiments with control samples containing no core. In the left figures for the Pd samples and in the right for the Pt samples. The error bar shows the standard deviation from a straight line in the Arrhenius plot.

4.3.1 Method for calculating activation energy

In figure 4.11 one can see both a typical readout from the mass spectrometer and the measured sample temperature in the reactor. The blue curve shows the ion current produced by CO_2 and the red curve shows the sample temperature. In this experiment CO was introduced after 9000 s and shortly thereafter one can see

that CO_2 signal is increasing. In the beginning there seems to be some overshoot of the signal before it starts decreasing towards some equilibrated state. A totally equilibrated state is though not fully reached and this will influence the estimation of the activation energy.
To estimate the activation energy one needs to know the reaction rate or at least something proportional to the reaction rate and one needs to know it at a few different temperatures. This we do have, the ion current produced by the CO_2 is proportional to the reaction rate and we measure the temperature of the sample. The ion current was though not stable and measuring the ion current shortly after the temperature rise, lets say at t=16500 s will differ from choosing to read it at t=18000s. This effects comes from the not reached equilibrium state. To decrease this effect and to measure only the effect of the temperature increase, the step height of the ion current at each temperature increase was used. That meaning, from the gray areas in figure 4.11, the minimum and the maximum values of the ion current was taken and the corresponding temperatures. The difference between the minimum and the maximum ion current was considered as the step height. Then, to obtain the temperature dependency, the initial ion current together with the temperature, just before increasing the temperature the first time was used as the first data point. The second data point consisted then of same ion current as the first data point plus the height of the first ion current step together with the temperature at the top of the ion current step. The third data point consisted of the ion current of the second data point plus the step height of the second ion current step together with the corresponding temperature. This procedure was repeated for all ion current steps and resulted in the data points used for fitting the Arrhenius equation.

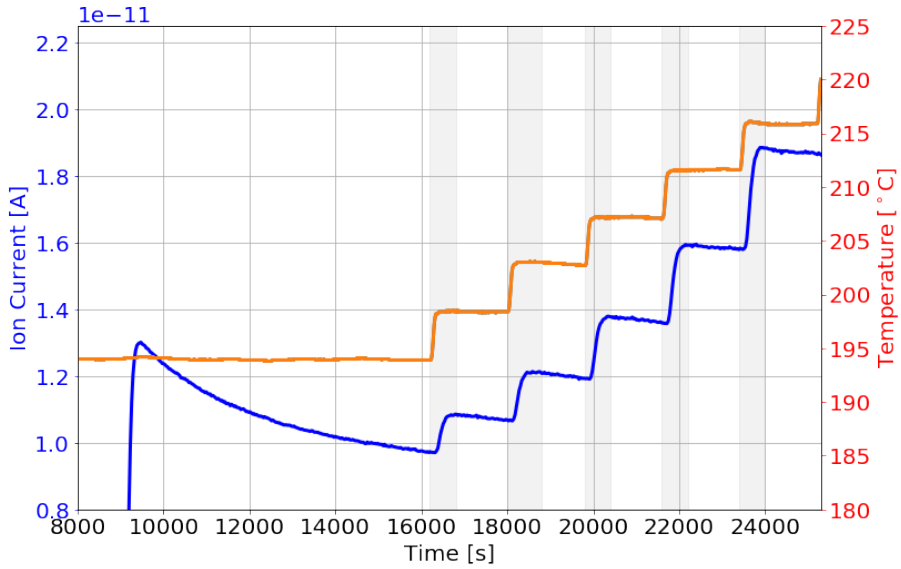

Figure 4.11: Temperature and ion current readout during a typical experiment. The red line shows the temperature and the blue line the ion current produced by CO_2.

5
Discussion

5.1 Reactor improvements

It was expected that introducing the pocket reactor in the flow reactor would increase the signal to noise ratio. The two orders of magnitude higher signal is a significant improvement and it allows for using smaller samples or far less active catalysts. The possibilities with the variable exhaust was not investigated in detail but could be used for controlling the flow rate at the sample. This could possibly be used for speeding up measurements, for example if one wants to introduce a new reaction condition with other gases in the reactor it takes some time before the old gases are flushed away. Opening the variable exhaust to the maximum could decrease this exchange time between two reaction conditions.
Furthermore there could be more improvements to the flow reactor. It is unnecessary big for the purpose of doing catalysis measurements and reducing the size would also decrease the exchange time between gases.

5.2 XPS and SEM for characterisation of samples, is it enough?

The XPS spectras confirms that all the samples has the expected species and the fact that the ratio between the intensity of Al2p peak and the Au_4f peak seems to correlate with the number of cycles of Al_2O_3 is nice. This could possibly be used as a measure of the shell thickness.
The high resolution peaks in the XPS spectras and the fitting in figure 4.4 shows that it is possible to characterise the chemical state of Pd. It needs though a very good signal from the XPS, which was difficult to obtain. Why this differed between measurements could have several causes. The pressure in the XPS chamber is one thing, a higher pressure would result in lower number of electrons reaching the detector. The focusing of the x-ray beam could have been too wide and sample spot used might have had less coverage of nanoparticles.
Nonetheless it shows that it is possible to quantify the chemical state composition of Pd. The possible increasing amount of oxides on the samples with more Al_2O_3 is an interesting finding. Why this is the case needs to be investigated further. Looking back to section 2.1.2, the electronic state is important for chemisorption of oxygen and a Fermi level equilibration resulting in a charge transfer between the core and the Pd could then be a factor.

There are though some uncertainties when it comes to the catalyst particles. The size of these are important to know, because it seems have an effect on the activation energy[23].

5.3 The origin of the different activation energies

There are a lot of activation energies reported for Pd and Pt nanoparticles but the range is large and there seems to be a dependency of both temperature and particle size[23, 24, 25]. All our experiments are though performed at the same temperature so that can be ruled out. The particle size is though an unanswered question that needs to be answered before comparing with literature values. The resolution of the obtained SEM images was not enough to calculate a size distribution and on the samples with less shell thickness we could not distinguish any Pd particles.
We can see that the activation energy of the samples containing no gold core differs a lot from the samples containing gold core, compare figure 4.8 and 4.9 with 4.10. This hints that we have some effect from the gold core. We do have an metal-insulator-metal structure and charge transfer between the core and the catalyst particles could be an explanation. This could be further investigated by changing the core material. A Pd core with Pd catalysts would not result in any Fermi level equilibration since they already have identical Fermi levels.

5.4 Using activation energy as a measure for CO oxidation

The use of Arrhenius equation on reactions that do not occur in gas phase has though been critiqued. With the main argument that the energy distribution among bound species is not represented by the Maxwell-Boltzmann distribution. This is summarised in an article [26] by Andrew K. Galwey and Michael E. Brown where also some justification of using Arrhenius equation to solid state kinetics is presented. The justification comes mainly from arguing that reactions involving phonons or electrons follows Bose-Einstein and Fermi-Dirac statistics respectively. Both of which can be approximated to an exponential energy term when describing the highest energies.
These arguments are probably both very valid but shows that the physics behind the reaction rate is not trivial and drawing conclusions from a single activation energy needs a deep understanding of the possible underlying mechanisms.
Besides this, there are some nice features that the use of Arrhenius equation gives. It is an easy measure, just fitting a straight line to some data points. It also does not really care about how much catalysts are present on the sample. This can be understood by looking at equation 2.3. Increasing the amount of catalysts by a factor of f would increase the reaction rate with the same factor and one ends up with

$$\frac{I}{p} = f \cdot A \exp\left(\frac{E_a}{k_b T}\right). \tag{5.1}$$

Taking the logarithm of this and rearranging the terms one gets

$$\ln(I) = -\frac{E_a}{k_b}\frac{1}{T} + \ln(p) + \ln(A) + \ln(f) \tag{5.2}$$

and one sees that the logarithm of the ion current is shifted to higher values but the slope is still the same. This makes it possible to compare activation energy from samples without having the exact same surface coverage of catalysts.
One should also understand that the activation energy do not necessarily tell anything about how good a catalyst is. It do describe how sensitive the reaction is to a change of temperature under the current reaction conditions.
The Arrhenius equation is though a widely used measure for catalysts which and it is easy to find values in the literature to compare with.

6

Conclusion and outlook

The modifications to the flow reactor improved the signal. This was expected, nonetheless the two order of magnitude better signal is a very good improvement. The variable exhaust could though be tested more.
The experiments on the core shell samples have yielded very interesting results, however there are still many unanswered questions. This report should though be seen more as an preliminary investigation than an attempt to answer several scientific questions. That meaning, it has instead of answered questions, actually created more of them.
The combination of the fact that the trends in the activation energy differs between the samples with gold core from the samples without gold core and the formation of more Pd oxides on samples with thicker Al_2O_3 suggests that we might have an effect of electron transfer between the core and the catalyst particles. The nature of the catalyst particles needs though to be characterised in greater detail. A size distribution would allow for comparing the activation energy values with values from literature.
To further investigate the possible effect of the core one could start with simplifying the system. Samples containing thin films instead of core shell nanoparticles would be easier to fabricate and could still have the metal-insulator-metal structure with gold, Al_2O_3 and Pd.
The core shell nanoparticles are though very interesting, the easy fabrication and the possibility of changing so many parameters makes them ideal for experiments. Their main asset is though the plasmonic nature of the core. This has not been utilised at all during these experiments. Tracking the plasmonic peak and shape during catalysis would yield more data about whats happening with the catalysts during reactions. It would also be a very good platform for investigating plasmon enhanced catalysis.

Bibliography

[1] Christopher Tiburski and Johan Tenghamn. ttlab: Analysis software for the most common physics lab equipment such as xps, mass spectrometer and optical spectroscopy. `https://pypi.org/project/ttlab/`, 2018–. [Online; accessed 2018-06-15].

[2] Well known expressions: "patience is a virtue". `https://www.bookbrowse.com/expressions/detail/index.cfm/expression_number/416/patience-is-a-virtue`. Accessed: 2018-08-25.

[3] Richard Rennie and Jonathan Law. *A Dictionary of Chemistry*. Oxford University Press, 2016.

[4] Julian RH Ross. *Heterogeneous catalysis: fundamentals and applications*. Elsevier, 2011.

[5] Kurt W Kolasinski. *Surface science: foundations of catalysis and nanoscience*. John Wiley & Sons, 2012.

[6] Paul L Houston. *Chemical kinetics and reaction dynamics*. Courier Corporation, 2012.

[7] Johannes W Niemantsverdriet. *Spectroscopy in catalysis: an introduction*. John Wiley & Sons, 2007.

[8] Yibin Bu, JW Hans Niemantsverdriet, and Hans OA Fredriksson. Cu model catalyst dynamics and co oxidation kinetics studied by simultaneous in situ uv–vis and mass spectroscopy. *ACS Catalysis*, 6(5):2867–2876, 2016.

[9] Iwan Darmadi. Nanofabrication for plasmon-mediated catalysis via absorption engineering. Master Thesis, Chalmers, 2016.

[10] Se H Oh and Edward J Bissett. Automotive applications of chemical reaction engineering and future research needs. In *Studies in Surface Science and Catalysis*, volume 159, pages 17–26. Elsevier, 2006.

[11] Matthijs A van Spronsen, Joost WM Frenken, and Irene MN Groot. Surface science under reaction conditions: Co oxidation on pt and pd model catalysts. *Chemical Society Reviews*, 46(14):4347–4374, 2017.

[12] Richard J Levy. Carbon monoxide pollution and neurodevelopment: a public health concern. *Neurotoxicology and teratology*, 49:31–40, 2015.

[13] Santosh K Upadhyay. *Chemical kinetics and reaction dynamics*. Springer Science & Business Media, 2007.

[14] Charles Kittel et al. *Introduction to solid state physics*, volume 8. Wiley New York, 1976.

[15] John G Simmons. Potential barriers and emission-limited current flow between closely spaced parallel metal electrodes. *Journal of Applied Physics*, 35(8):2472–2481, 1964.

[16] Elias Burstein and Stig Lundqvist. *Tunneling phenomena in solids*. Springer, 1969.

[17] Hans Fredriksson, Yury Alaverdyan, Alexandre Dmitriev, Christoph Langhammer, Duncan S Sutherland, Michael Zäch, and Bengt Kasemo. Hole–mask colloidal lithography. *Advanced Materials*, 19(23):4297–4302, 2007.

[18] Junhu Zhang, Yunfeng Li, Xuemin Zhang, and Bai Yang. Colloidal self-assembly meets nanofabrication: From two-dimensional colloidal crystals to nanostructure arrays. *Advanced materials*, 22(38):4249–4269, 2010.

[19] Peter E.'Sobol Kennetlf D. Bomben Jolm F. Moulder, William F. Stickle. *Handbook of X-ray Photoelectron Spectroscopy*. Perkin-Elmer Corporation, 1192.

[20] János Végh. The shirley-equivalent electron inelastic scattering cross-section function. *Surface science*, 563(1-3):183–190, 2004.

[21] Peter H Dawson. *Quadrupole mass spectrometry and its applications*. Elsevier, 2013.

[22] Gustaaf Van Tendeloo, Dirk Van Dyck, and Stephen J Pennycook. *Handbook of Nanoscopy, 2 Volume Set*. John Wiley & Sons, 2012.

[23] ZhaoWen Wang, Bin Li, MingShu Chen, WeiZheng Weng, and HuiLin Wan. Size and support effects for co oxidation on supported pd catalysts. *Science China Chemistry*, 53(9):2047–2056, 2010.

[24] Kyung I Choi and M Albert Vannice. Co oxidation over pd and cu catalysts iii. reduced al2o3-supported pd. *Journal of Catalysis*, 131(1):1–21, 1991.

[25] Boris V L'vov and Andrew K Galwey. Catalytic oxidation of co on platinum. *Journal of thermal analysis and calorimetry*, 111(1):145–154, 2013.

[26] Andrew K Galwey and Michael E Brown. Application of the arrhenius equation to solid state kinetics: can this be justified? *Thermochimica Acta*, 386(1):91–98, 2002.